Quantal and Non-Quantal Current and Potential Fields around Individual Sympathetic Varicosities on Release of ATP

M. R. Bennett,* L. Farnell,† W. G. Gibson,† Y. Q. Lin,* and D. H. Blair*

*The Neurobiology Laboratory, Institute for Biomedical Research, and Department of Physiology and the †School of Mathematics and Statistics, University of Sydney, Sydney, New South Wales 2006, Australia

ABSTRACT The electrical phenomena that occur at sympathetic varicosities due to the release of ATP include spontaneous and evoked excitatory junction potentials (SEJPs and EJPs; recorded with an intracellular electrode) as well as fast and slow excitatory junctional currents (EJCs; recorded with a loose-patch electrode placed over varicosities). The electrical analysis of these transients is hampered by lack of a detailed theory describing how current and potential fields are generated upon the release of a quantum of ATP. Here, we supply such a theory and develop a computational model for the electrical properties of a smooth muscle syncytium placed within a volume conductor, using a distributed representation for the individual muscle cells. The amplitudes and temporal characteristics of both SEJPs and fast EJCs are predicted by the theory, but those of the slow EJCs are not. It is shown that these slow components cannot arise as a consequence of propagation of fast quantal components from their site of origin in the muscle syncytium to the point of recording. The possibility that slow components arise by a mechanism of transmitter secretion that is different from quantal release is examined. Experiments that involve inserting peptide fragments of soluble *N*-ethylmaleimide-sensitive fusion attachment protein (α-SNAP) into varicosities, a procedure that is known to block quantal release, left the slow component of release unaffected. This work provides an internally consistent description of quantal potential and current fields about the varicosities of sympathetic nerve terminals and provides evidence for a non-quantal form of transmitter release.

INTRODUCTION

The paradigm organ for the study of sympathetic neuroeffector transmission is the vas deferens. The membrane potential changes during junctional transmission, the excitatory junction potentials (EJPs), were first recorded with an intracellular electrode in this muscle (Burnstock and Holman, 1961), as were the first measurements of the currents that flow during junctional transmission using extracellular loose-patch electrodes (Brock and Cunnane, 1987, 1988). However, it has been known for some time that identification of the factors that determine the characteristics of these potentials and currents depends, among other things, on knowledge of the electrical equivalent circuit of the smooth muscle syncytium (Bennett, 1972, 1973), the relation between the recording electrode and the site of quantal release in the syncytium (Bennett et al., 1993), the spatial relation between the sympathetic terminal varicosities and the smooth muscle cells in the syncytium (Bennett and Merrillees, 1966), and the stochastic nature of the interaction between the released quantum of transmitter and the underlying receptors (Bennett et al., 1995). It is not possible to examine quantal transmission at autonomic motor-nerve terminals without an understanding of the factors that determine the characteristics of the quantal potential and current (Bennett, 1996). Here we give a quantitative account of the fields generated in a smooth muscle syncytium, situated within a volume conductor, upon release of a quantum of transmitter at a site in the syncytium.

In the original description of quantal transmission at neuromuscular junctions, the excitatory transmembrane potential change (EJP) was shown to reach its peak in about 100 ms, but often cells were impaled that possessed EJPs with very fast components on the rising phase that resembled the spontaneous EJP (SEJP; see fig. 7 in Burnstock and Holman, 1961). Blakeley and Cunnane (1979) calculated the time derivative of the rising phase of EJPs and SEJPs recorded in the guinea-pig vas deferens. They found that the derivative of the EJP always contained a slow component (the *persistent* component) that lasted for about 80 to 100 ms, and occasionally contained a fast component (the *stochastic* component) that lasted for the order of 10 ms; for the SEJPs, only the fast component was found. These authors suggested that the fast intermittent stochastic component was due to the release of a quantum of transmitter onto the cell recorded from whereas the slow persistent component was due to the release of quanta onto surrounding cells, the results of which then radiated into the cell recorded from. Bennett and Gibson (1995), in a theoretical analysis of these observations, showed that they could not be accounted for by a model in which quantal release occurs from varicosities onto smooth muscle cells coupled together in an electrical syncytium; it is also necessary to have a relatively large number of small and slow currents generated in the syncytium in addition to the large and fast ones due to the release of a transmitter quantum. However, in contrast to the treatment given here, that analysis did not use a distributed representation for individual muscle cells in the syncytium,

Received for publication 10 July 2000 and in final form 30 November 2000.

Address reprint requests to Professor Max Bennett, Neurobiology Laboratory, Department of Physiology, University of Sydney, N.S.W. 2006, Australia. Tel.: 61-2-9351-2034; Fax: 61-2-9351 3910; E-mail: maxb@physiol.usyd.edu.au.

0006-3495/01/03/1311/18 $2.00

nor did it place the syncytium in a volume conductor. In addition, since the time of that analysis a large number of studies have been made of the extracellular currents that flow in smooth muscle during transmission (Bennett et al., 1998). We have, therefore, used the complete syncytial representation of the muscle to study both currents and potential generated in the muscle during transmission. The experimental observations, together with this theoretical analysis, support the conclusion that there is both quantal and non-quantal transmission at sympathetic nerve terminals.

METHODS

Theoretical

A discrete bidomain model of a smooth muscle syncytium

Early work (Bennett, 1972, 1973; Purves, 1976) modeled the smooth muscle bundle as a three-dimensional rectangular grid, with each node being a lumped representation of a muscle cell and the line joining these nodes representing the intracellular resistance (including the resistance of the gap junctions joining the cells). Later, this was extended to include the interstitial medium by introducing a second grid system, representing the region between the cells; these two grids were connected at every corresponding node by an RC circuit representing the membrane of a smooth muscle cell (Roth, 1992; Bennett et al., 1993). There is also a continuous version of the bidomain model, which dispenses with individual cells and treats the muscle tissue as two coupled continuous domains, one for the intracellular space and the other for the interstitial space. (For a review, see Henriquez, 1993).

In the present work the discrete approach will be adopted, following the work of Bennett et al. (1993). An extension of that work is that the muscle bundle is now assumed to be in a volume conductor and flow in this exterior region is modelled by extending the interstitial grid beyond the muscle surface. Another extension is the use of a distributed representation for some of the cells.

For the purposes of developing a mathematical model, smooth muscle tissue is assumed to be made up of a regular three-dimensional array of parallel cylindrical cells of length ℓ and diameter d. Three-dimensional cartesian coordinates x, y, and z are introduced such that the muscle tissue occupies the region $z \geq 0$ and the longitudinal axis of each cell is parallel to the y–axis. Fig. 1 $A(a)$ shows several such cells, and Fig. 1 $A(b)$ gives the

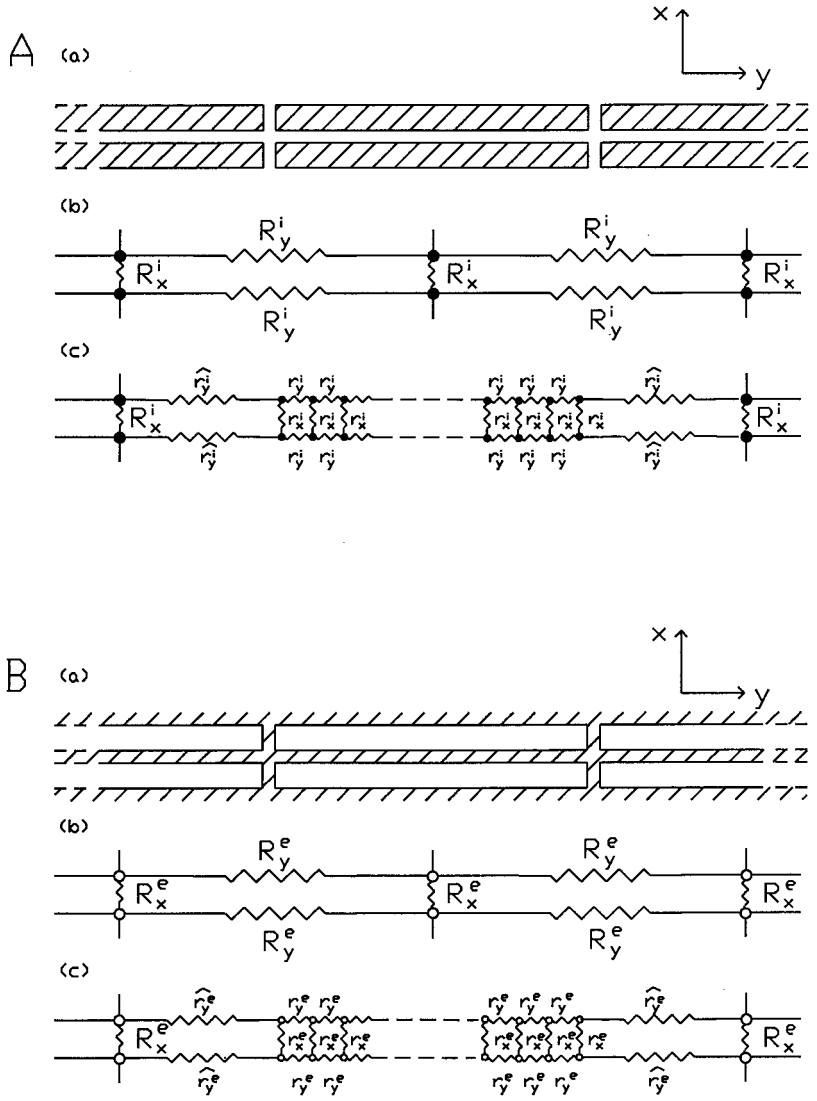

FIGURE 1 The smooth muscle syncytium. A(a) shows several smooth muscle cells as cylinders of length ℓ and diameter d stacked in a regular array. A(b) shows the equivalent circuit for the interiors of these cells when a single lumped representation is used for each cell. Each filled node represents a point in the interior of a smooth muscle cell, R_y^i is the sum of the longitudinal cytoplasmic resistance of a cell plus the resistance of the gap junction between the ends of two cells and R_x^i is the resistance due to transverse coupling by gap junctions parallel to the x-axis (a similar coupling occurs in the z-direction). A(c) shows the method of introducing a distributed representation for the central cells; each single node is replaced by n nodes coupled as shown, the new resistances $\hat{r}_y^i$, r_y^i, and r_x^i being chosen so that the overall resistance of the distributed model is equal to that of the lumped model. B, shows the corresponding model for the interstitial medium. Each open node represents a point lying just outside a smooth muscle cell.

corresponding lumped representation for the cell interiors, with each filled node representing a single cell. The cells are connected by gap junctions and these are assumed to join cells longitudinally at the ends and also transversely. The longitudinal intracellular resistance R_y^i (Ω) comprises the cytoplasmic resistance of two half-cells plus the resistance of the gap junction between them. Thus

$$R_y^i = R^{cyto} + R_{long}^{gap}, \tag{1}$$

where R^{cyto} (Ω) is the cytoplasmic resistance in the longitudinal direction of a single cell and R_{long}^{gap} (Ω) is the resistance of the gap junction joining their ends. In the transverse directions the corresponding resistances are

$$R_x^i = R_z^i = R_{trans}^{gap}, \tag{2}$$

where R_{trans}^{gap} (Ω) is the total resistance due to gap junctions in the transverse directions parallel to either the x- or z-axis. (The small transverse contribution from the cytoplasm has been neglected, since $d \ll \ell$.)

Fig. 1 *B*(*a*) and (*b*), shows the corresponding model for the space between the cells. If ρ_e (Ω cm) is the resistivity of the interstitial fluid and f_i is the fraction of total cross-sectional area in the muscle bundle occupied by intracellular space, then (Cole and Curtis, 1950; Henriquez, 1993)

$$R_y^e = \rho_e \frac{f_i}{1-f_i}\frac{\ell}{\sigma}, \tag{3}$$

$$R_x^e = R_z^e = \rho_e \frac{1+f_i}{1-f_i}\frac{1}{\ell}, \tag{4}$$

where $\sigma = \pi(d/2)^2$ is the cross-sectional area of the cell. Note that if D denotes the transverse internodal spacing then $f_i = \pi(d/2)^2/D^2$, so $D = \sqrt{\pi/f_i}(d/2)$. The modeling indicated in Figs. 1 *A*(*b*) and 1 *B*(*b*) is extended to the whole muscle bundle, giving two three-dimensional grids that occupy the same space, as shown in Fig. 2 *A*. Both grids extend indefinitely in the x and y directions, but whereas the intracellular grid (filled nodes joined by solid lines) stops at the surface $z = 0$, the interstitial grid (open nodes joined by broken lines) continues into the extracellular region $z < 0$. For computational convenience, the same internodal spacing is used there so that the extracellular resistances are given by

$$R_y^o = \rho_o \frac{\ell}{\sigma}, \tag{5}$$

$$R_x^o = R_z^o = \rho_o \frac{1}{\ell}, \tag{6}$$

where ρ_o (Ω cm) is the resistivity of the extracellular fluid.

The transmembrane coupling, between the intracellular and interstitial media at each node, is represented by an RC circuit with resistance R_m (Ω) and capacitance C_m(F), these values being the same for all nodes (Fig. 2 *B*).

Equations for the potentials

Let the nodes of the grids shown in Fig. 2 *A* be labelled by the rectangular Cartesian coordinates (i, j, k) where i, j, k take integer values with $-\infty < i, j, k < \infty$, with $k \geq 0$ corresponding to the muscle tissue and $k < 0$ to the extracellular space. At node (i, j, k), $k \geq 0$, let V_{ijk}^i (V) denote the intracellular potential (or, more precisely, its deviation from resting potential), V_{ijk}^e (V) the interstitial potential and I_{ijk} (A) the current flowing across the cell membrane from the intracellular to the interstitial space (Fig. 2 *B*). At node (i, j, k), $k < 0$, let V_{ijk}^o (V) denote the extracellular (i.e., exterior) potential.

Conservation of intracellular current at node (i, j, k), $k \geq 0$, gives

$$-I_{ijk} + \left(\frac{1}{R_x^i}D_x^2 + \frac{1}{R_y^i}D_y^2 + \frac{1}{R_z^i}D_z^2\right)V_{ijk}^i = 0, \tag{7}$$

where $\mathbf{R}^i = (R_x^i, R_y^i, R_z^i)$ (Ω) are the resistances between two neighboring intracellular nodes and we have introduced the notation

$$\begin{aligned} D_x^2 V_{ijk}^i &= V_{i+1jk}^i + V_{i-1jk}^i - 2V_{ijk}^i, \\ D_y^2 V_{ijk}^i &= V_{ij+1k}^i + V_{ij-1k}^i - 2V_{ijk}^i, \\ D_z^2 V_{ijk}^i &= V_{ijk+1}^i + V_{ijk-1}^i - 2V_{ijk}^i. \end{aligned} \tag{8}$$

Similarly, conservation of interstitial current at node (i, j, k), $k \geq 0$, gives

$$I_{ijk} + \left(\frac{1}{R_x^e}D_x^2 + \frac{1}{R_y^e}D_y^2 + \frac{1}{R_z^e}D_z^2\right)V_{ijk}^e = 0. \tag{9}$$

At node (i, j, k) in the extracellular region ($k < 0$) the corresponding equation is

$$\left(\frac{1}{R_x^o}D_x^2 + \frac{1}{R_y^o}D_y^2 + \frac{1}{R_z^o}D_z^2\right)V_{ijk}^o = 0. \tag{10}$$

The membrane current at node (i,j,k) is (Fig. 2B)

$$I_{ijk} = C_m \frac{dV_{ijk}^m}{dt} + \frac{1}{R_m}V_{ijk}^m - I_{in}(t)\delta_{(ijk)(pqr)}, \tag{11}$$

where $V_{ijk}^m = V_{ijk}^i - V_{ijk}^e$ is the membrane potential at node (i, j, k). The final term on the right hand side mimics the effects of transmitter release at node (p, q, r) [$\delta_{(ijk)(pqr)} = 1$ if $(ijk) \equiv (pqr)$ and is zero otherwise]; it corresponds to a current $I_{in}(t)(A)$ being injected at node (p, q, r) in the intracellular space and an equal current being removed at node (p, q, r) in the interstitial space. If there is release onto more than one node then a term for each such node is to be included on the right hand side of Eq. 11. The form chosen for $I_{in}(t)$ is a double exponential:

$$I_{in}(t) = I_0(e^{-\alpha t} - e^{-\beta t}), \tag{12}$$

where I_0, α, and β are constants. Substituting Eq. 11 into Eqs. 7 and 9 gives two coupled equations for the potentials V^i and V^e.

Boundary conditions

It is assumed that initially there is no electrical activity in the muscle tissue, so

$$V_{ijk}^i = 0, \quad V_{ijk}^e = 0, \quad V_{ijk}^o = 0, \quad \text{for all } i, j, k, \quad \text{when } t = 0. \tag{13}$$

Also, the potential will remain at zero at the distant boundaries:

$$\begin{aligned} V_{ijk}^i \to 0, \quad V_{ijk}^e \to 0, \quad &\text{as } i \to \pm\infty, \quad j \to \pm\infty, \quad k \to +\infty, \\ V_{ijk}^o \to 0, \quad &\text{as } i \to \pm\infty, \quad j \to \pm\infty, \quad k \to -\infty. \end{aligned} \tag{14}$$

At the surface $z = 0$, because the muscle cells do not extend into the region $z < 0$, the z-component of the intracellular current must vanish. In the discrete model, this is implemented as

$$V_{ij-1}^i = V_{ij0}^i, \quad \text{for all } i, j, \tag{15}$$

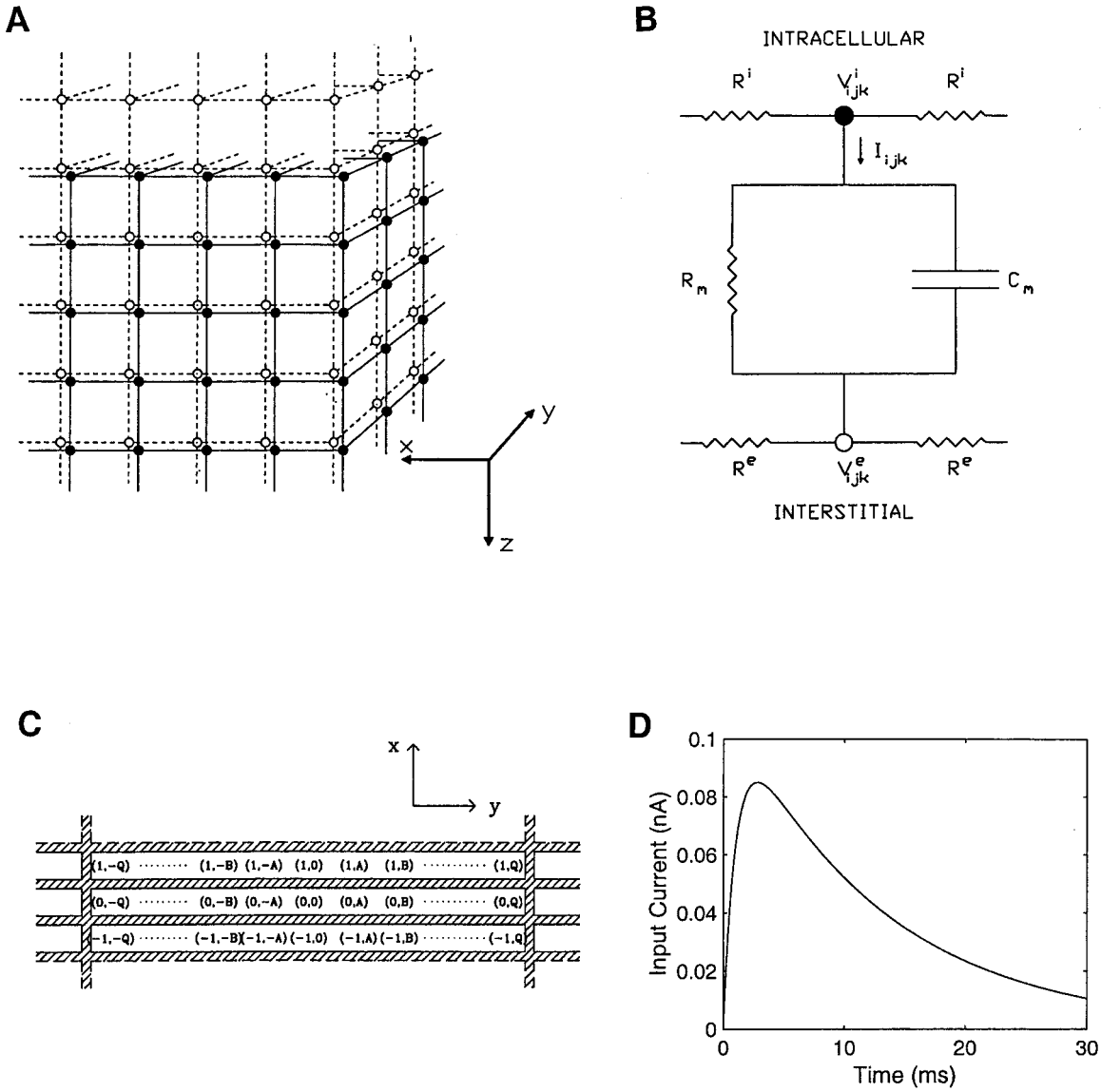

FIGURE 2 *A* shows the two grids representing the smooth muscle syncytium when the lumped representation of Fig. 1 *A*(a) and *B*(b) is used. The *x*- and *z*-axes are in the transverse plane of the muscle and the *y*-axis is along the longitudinal axis of the muscle. Each filled node represents a point within a single muscle cell, coupled to six other cells as indicated by the solid lines. Each open node represents a point lying just outside a single smooth muscle cell, coupled to similar points outside six other cells in the same configuration as that for the inside points, each coupling being represented by a broken line. Each of the intracellular nodes is coupled to adjacent interstitial node by the parallel resistance and capacitance of the cell membrane. (Note that only a few nodes and their connections have been drawn; also, mathematically the open and closed nodes are coincident at the same point in space; they have been drawn separated for clarity.) Theoretically, both grids are infinite in the *x*- and *y*-directions; the intracellular grid occupies the region $z > 0$ with the plane $z = 0$ being the muscle surface; the interstitial grid continues into the region $z < 0$, where it now represents the extracellular medium. *B* shows the equivalent circuit for the transmembrane connection between an intracellular and an interstitial node. The circuit connects each filled node in *A* to its adjacent open node and thus each overall node consists of this circuit, representing a single lumped cell. R_m and C_m are the membrane resistance and capacitance, I_{ijk} is the membrane current, V^i_{ijk} is the deviation of the intracellular potential from its resting value, V^e_{ijk} is the interstitial potential and R^i and R^e the intracellular and interstitial resistances. Only the one-dimensional case is illustrated; in the three-dimensional case there will be six such resistances at each node and these can take different values in the *x*-, *y*-, and *z*-directions. *C* shows the nomenclature used to designate the coordinate system of the syncytium. The lumped cells are labelled by their nodal coordinates (i, j, k) where i, j, k take integer values. The n locations on the central block of cells having a distributed representation are labeled by giving j the intermediate values $\ldots, -B, -A, 0, A, B, \ldots$ for each such cell. The figure shows three such cells, with locations labelled (i, j) (k has been suppressed) for the case $n = 35$. *D* shows the current injected at a node of the syncytium for simulating the effect of an ATP quantum.

where an extra layer of dummy intracellular nodes (corresponding to $k = -1$) has been introduced. At the muscle surface the interstitial space becomes extracellular space and the z-component of current flow between these spaces is continuous (Krassowska and Neu, 1994). This is implemented by making the extracellular and the interstitial potentials agree at nodes on the plane $z = 0$ and also at nodes immediately above and below it:

$$V^{e}_{ijk} = V^{o}_{ijk}, \quad \text{for all } i, j, \quad \text{and } k = -1, 0, \text{and } 1. \tag{16}$$

Method of solving for the potentials

In most previous treatments of the bidomain model, both the discrete and continuous versions, the equations have been uncoupled and the problem reduced to that of solving one differential equation for the membrane potential. In the infinite medium this uncoupling is possible if the anisotropy in the intracellular and the interstitial regions is assumed to be identical. In the present case, this means

$$\frac{R^{e}_{x}}{R^{i}_{x}} = \frac{R^{e}_{y}}{R^{i}_{y}} = \frac{R^{e}_{z}}{R^{i}_{z}}. \tag{17}$$

For a finite medium with one or more boundaries, uncoupling is still not possible even if Eq. 17 holds. This is because the different boundary conditions on V^{i} and V^{e} (Eqs. 15 and 16) prevent the equations from being uncoupled. (The treatment given in Bennett et al. (1993) allowed uncoupling by neglecting the extracellular field and imposing an unrealistic boundary condition on V^{e}.)

In the present case, we wish to retain the correct boundary conditions, Eqs. 15 and 16, and also to avoid the unrealistic assumption of equal anisotropy ratios specified by Eq. 17. This means that the equations for V^{i} and V^{e} do not uncouple and must be solved simultaneously. A solution can be achieved by recasting the equations in matrix form. Introduction of the column vector

$$U_{ijk} = \begin{pmatrix} V^{i}_{ijk} \\ V^{e}_{ijk} \end{pmatrix} \tag{18}$$

allows Eqs. 7, 9, and 11 to be combined (compare Henery et al., 1997) as

$$C_{m}\frac{d}{dt}(JU_{ijk}) + \frac{1}{R_{m}}(JU_{ijk}) = (K_{x}D^{2}_{x} + K_{y}D^{2}_{y} + K_{z}D^{2}_{z})U_{ijk} + I(t)L\delta_{(ijk)(pqr)}, \tag{19}$$

where

$$J = \begin{pmatrix} 1 & -1 \\ 1 & -1 \end{pmatrix}, \quad L = \begin{pmatrix} 1 \\ 1 \end{pmatrix}, \tag{20}$$

and

$$K_{x} = \begin{pmatrix} 1/R^{i}_{x} & 0 \\ 0 & -1/R^{e}_{x} \end{pmatrix}, \quad K_{y} = \begin{pmatrix} 1/R^{i}_{y} & 0 \\ 0 & -1/R^{e}_{y} \end{pmatrix}, \quad K_{z} = \begin{pmatrix} 1/R^{i}_{z} & 0 \\ 0 & -1/R^{e}_{z} \end{pmatrix}. \tag{21}$$

Eq. 19 is a single equation for the vector U_{ijk}. It can be solved by standard methods; in particular, an explicit method which combines a finite difference scheme centered in time with a method of updating on a staggered mesh has been found to give good stability and reasonable run times (see Appendix in Henery et al., 1997, for details). The extracellular potential V^{o} is readily included in the computation scheme, using Eqs. 10 and 16. In practice, a system of finite size must be simulated and the limits $-45 \le i \le 45$, $-15 \le j \le 15$, $-55 \le k \le 45$, where (i,j,k) is the node label, were found to be sufficient to give solutions independent of the boundary position. A time step of 0.05 μs was used.

Calculation of the extracellular current measured by an electrode

The extracellular loose patch electrode is modeled as a right circular cylinder with its axis parallel to the z-axis and its tip in the $z = 0$ plane. The walls of the electrode are modelled by setting the appropriate resistances in the extracellular space to very high values. The capacitance of the electrode was not taken into account, as it is not expected to significantly distort the signal. (See Bennett et al. (1997) for a calculation of the distorting effect of a loose patch electrode; that calculation was for a faster signal, so the effect will be smaller in the present case.) The total current flowing across the circumference of the tip is calculated as the algebraic sum of the currents in all the resistances in the plane $z = 0$ that cross the electrode tip. Thus the total current measured by the electrode is taken to be

$$I_{e} = \sum \frac{\Delta V^{o}}{R_{grid}}, \tag{22}$$

where $\Delta V^{o} = V^{o}_{inside} - V^{o}_{outside}$ is the difference in the extracellular potential between two contiguous nodes in the $z = 0$ plane, R_{grid} is the resistance between these nodes and the sum is over all grid lines cut by the circumference of the tip.

A distributed representation for single smooth muscle cells

The above treatment uses a single lumped representation for each smooth muscle cell. Provided one is interested only in intracellular potentials or membrane potentials, this is a reasonable approximation, since the interior of a cell will quickly become isopotential. However, it clearly does not give an accurate representation of extracellular current flow since muscle cells are the order of 200 μm long and this will give rise to a spatial distribution of current flow that cannot be reproduced in detail by the above lumped model. Since the loose patch electrode has a diameter of about 12 μm or less, this neglect could be significant.

In order to investigate this further, a distributed representation has been introduced for those muscle cells in the vicinity of the electrode tip. Specifically, each cell that was previously replaced by a single node in the plane $y = 0$ is now replaced by n nodes, where n is an odd integer (Fig. 1 *A*(c)). The longitudinal resistances r^{i}_{y} between these new nodes are due to the cytoplasm only, so

$$r^{i}_{y} = \frac{1}{n}R^{cyto}. \tag{23}$$

The end resistances $\hat{r}^{i}_{y}$ include the gap junction, so

$$\hat{r}^{i}_{y} = R^{gap}_{long} + \left(\frac{1}{2} + \frac{1}{2n}\right)R^{cyto}. \tag{24}$$

(Since $\hat{r}^{i}_{y} + ((n-1)/2)r^{i}_{y} = R^{i}_{y}$, this gives the same overall resistance as before.) The new transverse resistances, r^{i}_{x} and r^{i}_{z}, are given by

$$r^{i}_{x} = r^{i}_{z} = nR^{gap}_{trans}. \tag{25}$$

A similar distributed representation is introduced for the corresponding interstitial regions (Fig. 1 *B*(c)), with

$$r^{e}_{y} = \frac{1}{n}R^{e}_{y} \tag{26}$$

$$\hat{r}_y^e = \left(\frac{1}{2} + \frac{1}{2n}\right) R_y^e \tag{27}$$

$$r_x^e = r_y^e = nR_x^e. \tag{28}$$

This distributed representation is also extended to the extracellular region, for all those nodes previously in the plane $y = 0$. The other modification that must be made is that the new intracellular and interstitial nodes are to be joined by *RC*-circuits, similar to that shown in Fig. 2 *B*, only now each resistance is nR_m and each capacitance is C_m/n.

The nomenclature used to specify positions in the syncytium when some cells have a distributed representation is shown in Fig. 2 *C*. Note that even with this distributed representation the position of the ends of the cells remains blurred, since $\hat{r}_y^i$ still lumps half the cytoplasmic resistance of the next cell with the longitudinal gap junction resistance. However, this is of no practical importance since the loose-patch electrode is always taken to lie completely within the distributed representation area.

Properties of the quantal current

Loose patch recordings have been made of the current field due to the release of ATP quanta from visualized varicosities located in strings running on the surface of the muscle before they penetrate into the media (Lavidis and Bennett, 1992, 1993). In order to interpret these loose patch recordings a theory has been developed that allows for an analysis of them in terms of the contributions to the quantal potential field (V_e) arising from quantal release at varicosities throughout the syncytium. To this end, a quantum of ATP has been taken as generating a current of the kind shown in Fig. 2 *D*. The characteristics of this quantal current are that it possesses an average time-to-peak of 2.8 ms and a 10% to 90% rise time of 1.5 ms with an average exponential time of decay (τ) of 12.5 ms (see fig. 8 in Bennett et al., 1995). The peak amplitude of the ATP quantal current is about 100 μV, equivalent to 100 pA for a loose patch recording electrode resistance of 1.0 MΩ (see fig. 4A in Bennett et al., 1995). A current of 76 pA is generated by about 1000 molecules of ATP on a patch of receptors of density between 100 μm^{-2} to 1000 μm^{-2} (fig. 7A in Bennett et al., 1995). For a 1 μm^2 size receptor patch of P_{2x1} receptors found beneath junctional varicosities in the vas deferens (see Barden et al., 1999), that is one of diameter about 1.12 μm, and with the distance separating the varicosity and postjunctional membrane of 50 nm (see Cottee et al., 1994), the rise time (T_p: 10% to 90% of the peak value) of the quantal current ranges stochastically between one and two ms (with a standard deviation of 0.5 ms). The decay time constant is between 9 ms and 16 ms (see table 1 in Bennett et al., 1995). The current shown in Fig. 2 *D* therefore has characteristics comparable to those expected on both experimental and theoretical grounds.

Parameter values

The parameter values used in the calculations are shown in Table 1.

The membrane capacitance was chosen to give a time constant $\tau = R_m C_m$ of 300 ms. The longitudinal cytoplasmic resistance of a typical smooth muscle cell is about 50 MΩ and this is also approximately the resistance of a gap junction between cells (Brink, 1998). Thus $R^{cyto} = 50$ MΩ and, assuming cells are longitudinally coupled by a single gap junction, $R^{gap}_{long} = R^{gap} = 50$ MΩ. Assuming that there is also the equivalent of one gap junction between cells in each transverse direction, then $R^{gap}_{trans} = R^{gap} = 50$ MΩ. The values for $\mathbf{R}_i$ given in Table 1 then follow from Eqs. 1 and 2. Using $\rho_e = \rho_o = 100$ Ωcm, $f_i = 0.7$, $d = 4$ μm, and $\ell = 200$ μm in Eqs. 3–6 gives the values for $\mathbf{R}^e$ and $\mathbf{R}^o$ in Table 1. As there is some uncertainly in the values for $\mathbf{R}^i$ and $\mathbf{R}^e$, a number of calculations were performed in which these were varied over a wide range about the values given in Table 1. Although this led to some quantitative changes in the results, these were not sufficient to alter the main findings; in particular, rise times of intracellular potentials and extracellular currents measured by a loose patch electrode were found to vary by only small amounts when $\mathbf{R}^i$ and $\mathbf{R}^e$ were changed. For the distributed representation, once a value for n has been chosen, the appropriate resistances follow from Eqs. 23–28. A sequence of calculations of the electrode current using increasing values of n indicated that by $n = 35$ results had stabilized so this value was then used in all calculations.

Experimental

Electrophysiology

All experiments were performed on the vas deferens of mice (strain Balb/c), 5 to 6 weeks old. Animals were anesthetized with halothane, then killed by cervical fracture. Both vasa deferentia were dissected free along with the connective tissue containing the hypogastric nerves. The tissue was then placed in a 3-ml capacity Perspex chamber, pinned through the epididymal end to a sheet of Sylgard in the bottom of the chamber, and immersed in a modified Tyrode's solution (mM) of Na^+, 136.9; K^+, 2.7; Mg^{2+}, 1.0; Cl^-, 140.5–143.3; $(H_2PO_4)^-$, 1.3; $(HCO_3)^-$, 14.9; Ca^{2+}, 2.0; glucose, 7.8; and nifedipine, 10 μM, continuously bubbled with 95% O_2 and 5% CO_2 to maintain the pH between 7.1 and 7.4. The tissue chamber was continuously perfused with warm (30–33°C) solution.

The prostatic end of the vas deferens was gently sucked into pipette filled with modified Tyrode solution. A silver/silver chloride wire on the inside of the pipette and one on the outside were used to stimulate the axons running on the surface of the mouse vas deferens, using square wave pulses of 0.05 to 0.08 ms duration and 8 to 16 V amplitude generated by Grass S48 Stimulator (Quincy, MA.). The axons were stimulated contin-

TABLE 1 Values of parameters used

Quantity	Symbol	Value	Reference
Junctional current (Eq. 12)	I_0	116 pA	See text
	α	0.08 ms^{-1}	See text
	β	0.97 ms^{-1}	See text
Membrane resistance	R_m	3.6×10^9 Ω	Bennett (1973)
Membrane capacitance	C_m	8.4×10^{-11}F	See text
Cytoplasmic resistance	R^{cyto}	50×10^6 Ω	Brink (1998)
Gap junction resistance	R^{gap}	50×10^6 Ω	Brink (1998)
Intracellular resistance	$\mathbf{R}^i$	$(50, 100, 50) \times 10^6$ Ω	See text
Interstitial resistance	$\mathbf{R}^e$	$(0.03, 38, 0.03) \times 10^6$ Ω	See text
Extracellular resistance	$\mathbf{R}^o$	$(0.005, 15.9, 0.005) \times 10^6$ Ω	See text
Cell diameter	d	4 μm	Brink (1998)
Cell length	ℓ	200 μm	Brink (1998)

ually at 0.2 Hz while searching for the extracellular signal of nerve terminal impulses and the excitatory junction current (EJC).

Borosilicate glass capillaries (1.5 mm O.D. × 0.86 mm I.D., Clark Electromedical Instruments, Kent, England) were used for preparation of microelectrodes. The microelectrodes, with tip diameter about 2 μm, were pulled with a Brown-Flaming Micropipette Puller (Model P-87, Sutter Instrument Co., San Rafael, CA). To obtain good seal during the recording, the loose-patch electrodes were bevelled on Micropipette Beveler to about 30–35 degrees (Model BV-10, Sutter Instrument Co.) until the diameter of the tip reached about 12 μm.

Data were collected and stored on a 7600/120 PowerMacintosh computer via Maclab/4S interface (ADInstruments, Castle Hill, Australia.) and the analyses were performed with the software Igor Pro 3.0. (WaveMetrics Inc., Lake Oswego, OR) and DeltaGraph 4.0.5. (SPSS Inc., Chicago, IL).

Visualisation of varicosities

Varicosities were visualized essentially as described in Lavidis and Bennett (1993). Briefly, the preparation was left in the recording bath in the modified Tyrode solution for at least 60 minutes to ensure that nifedipine could take effect. It was bathed for 30 s in 3.3 diethyloxardicarbocyanine iodide (0.1 m; DiOC2(5)), then washed with modified Tyrode solution for 3 min. Terminals were chosen by viewing the DiOC2(5)-fluorescent image via an image intensifier camera (Panasonic) attached to an Olympus (BH2) microscope equipped with rhodamine filter set and the image was then displayed on a video monitor (Panasonic). Varicosities were also visualized by orthograde transport of rhodamine conjugated to dextran down the cut sympathetic nerves into their terminals (Bennett et al., 1998). This transport took 2 to 3 hours before the varicosities could be visualized.

Once terminals were chosen, their location was marked on the monitor then an electrode was placed over that region of the preparation under bright field microscopy. Images were acquired with a frame grabber card (Scion Corporation, Frederick, Maryland) in a 7600/120 Power Macintosh computer running NIH Image software, which can be found at http://rsb.info.nih.gov/nih-image.

Introduction of α-SNAP peptides into varicosities

The α-SNAP peptide (C-KGFLS SLFGG SSK) was chosen to block quantal transmitter release, as it was previously shown to inhibit release at the squid giant axon (DeBello et al., 1995). The peptides were chemically synthesized with a terminal cysteine residue to allow disulfide conjugation with a vector peptide (penetratin: C-RQIKI WFQNR RMKWK K; Prochiantz, 1999). Penetratin itself was synthesized with a nitropyridine-modified terminal cysteine to prevent homodimerization. For conjugation, peptides were dissolved in acetate buffer (200 mM, pH 4.0), then mixed with a threefold excess of penetratin and incubated at 30°C for 1 hour. Heterodimer conjugates were then purified from unconjugated and homodimerized peptide by reverse phase HPLC and confirmed with electrospray mass spectroscopy. Purified conjugate was then lyophylized and redissolved in mouse Ringer's solution at 100 μM; aliquots were stored at −20°C until use.

RESULTS

Theoretical quantal potential fields at a varicosity in a muscle syncytium

The theoretical intracellular (V_i) and extracellular (V_e) quantal potential fields generated by current flow simulating the release of a quantum of ATP at different depths (z) in the syncytium are shown in Fig. 3, *A* and *B*, respectively. The spatial distribution of the fields is indicated at the time of peak current flow due to the release of a quantum at the different depths in the syncytium indicated. Note that the field for each individual V_i is symmetrical along the z-axis for quanta released deep in the syncytium ($i = 0, j = 0, k = 3$; henceforth (0, 0, 3)); closer to the surface the peak V_e field decreases although the peak V_i field increases near the surface apposing the volume conductor (Fig. 3). The extracellular field is extremely small, only about 15 μV, and is very unlikely to be recorded with a sharp electrode in the way in which the much larger fields generated by the release of a quantum of acetylcholine are at the motor endplate (Bennett et al., 2000). For this reason, loose patch electrodes must be used in order to be able to concentrate the quantal current lines under the electrode and so amplify the extracellular potentials generated by the ATP quantum.

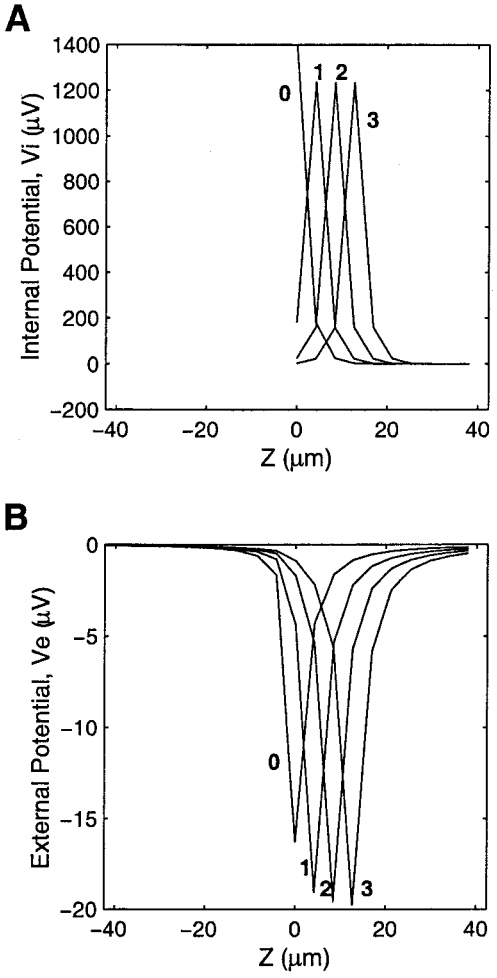

FIGURE 3 Theoretical variation of the amplitude in the z-direction of the internal (intracellular) potential field V_i (*A*) and the external (interstitial) potential field V_e (*B*), at (0, 0, z) at the time of peak current current flow. This is due to current injection simulating the release of a quantum of ATP from a varicosity located at different depths in the muscle syncytium. The releases at nodes located in the z direction at $k = 0$ (surface), 1, 2, and 3, respectively, are indicated. The current injection is given in Fig. 2 *D*.

The effect of such loose patch electrodes placed over a source on the extracellular potential fields is shown in Fig. 4. Equipotential contour lines of V_e show how these are compressed for a loose patch electrode of 12 μm diameter placed with its center at (0, 0, 0): the potential lines in the volume conductor reach values of magnitude about 3 μV at the immediate inside of the electrode for the case of a quantal release at (0, 0, 0) (compare Fig. 4 *B*, top panel, with Fig. 4 *A*, top panel; in *B* the contour labeled 1, corresponding to -3 μV, is contained within the electrode). In the case of a quantal release at (0, 0, 3), the potential lines at the surface of the muscle (0, 0, 0) within the loose patch electrode only reach values of magnitude 1 μV (Fig. 4 *B*, bottom panel; the contour labeled 2, corresponding to -1 μV, is now within the electrode tip).

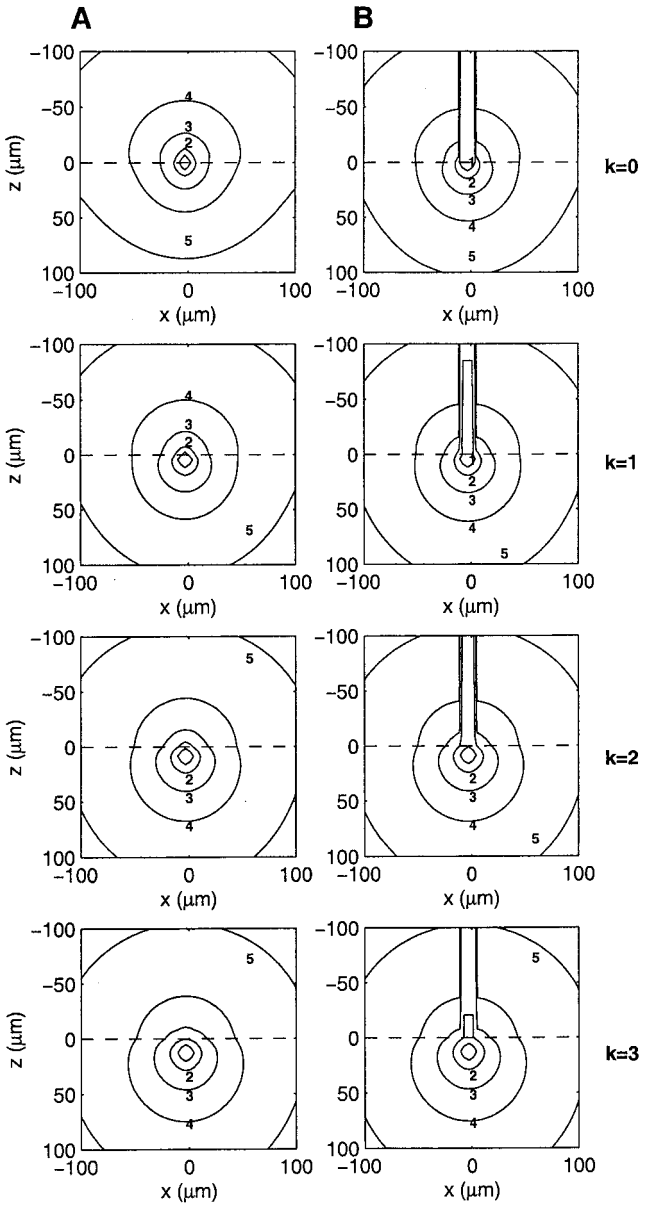

FIGURE 4 Theoretical variation of the quantal potential field amplitude (V_e) in the *xz*-plane at $y = 0$ at the time of peak current flow due to current injection simulating the release of a quantum of ATP at different depths (z) in the muscle syncytium. These releases occurred at nodes located in the z-direction at $k = 0$, 1, 2, and 3, respectively, (as indicated to the right of the figure) in the absence (*A*) and presence (*B*) of a loose patch electrode with center at at (0, 0, 0). In each panel, the broken horizontal line indicates the surface $z = 0$. The current injection had the properties of that given in Fig. 2 *D* and the loose patch electrode was 12 μm in diameter. The numbers 1 to 5 on the contour lines indicate, respectively, the following potentials: -3 μV, -1 μV, -0.3 μV, -0.1 μV, and -0.03 μV.

Theoretical current fields at a varicosity in a muscle syncytium

In order to determine the voltages recorded with the loose patch electrode, it is necessary to sum the total current flow passing between the electrode tip, usually taken as being situated at (0,0,0), and the surface of the tissue, giving the electrode current I_e as calculated from Eq. 22. Fig. 5 *A* shows the electrode current for quantal releases at node (0,0,k) for $k = 0$, 1, 2, 3, and 4; that is, for releases onto muscle cells at these different depths beneath the electrode. The peak amplitude of the electrode current falls off exponentially with z, so that by one node deep (corresponding to $z = D \approx 4.24$ μm; see Methods) only 1/e of the current appears under the electrode compared with that for quantal release at $z = 0$ (Fig. 5 *E*). One feature of these curves is the extent to which the time to peak of the electrode current at the surface remains relatively constant as the source of the quantal release is moved along the z-axis. This is best illustrated by normalising the peak electrode currents for quantal releases at different depths in the syncytium to that for release at the surface (0,0,0), as shown in Fig. 5 B: by 4 nodes deep (≈ 17 μm) the time to peak has only increased by about 0.15 ms over the value of 1.57 ms for $z = 0$ (Fig. 5 F).

It is well established that currents arising outside the electrode tip at the surface of the tissue give rise to a current flow at the tip, which is the reverse of that for currents arising within the electrode (Bennett et al., 1993). However, the question arises as to the direction of electrode current flow (and hence potential) when quantal release does not occur at the surface nor at sites that are immediately under the electrode along the z-axis. Fig. 5 shows examples of the electrode currents when a quantal release occurs at node (i, 0, 1) for different values of i (Fig. 5 *C*) and at (0, j, 1) for different values of j (Fig. 5 *D*); for movements in the x-direction more than one site displaced from (0, 0, 0) the electrode current is at least an order of magnitude smaller than the electrode current due to release at (0, 0, 0) (compare Fig. 5 *C* with Fig. 5 *A*); for movements in the y-direction more than two distributed nodes from (0, 0, 0) the peak current is at least an order of magnitude smaller than that at (0, 0, 0) (compare Fig. 5 *D* with Fig. 5 *A*). If consideration is given to quantal release at another muscle

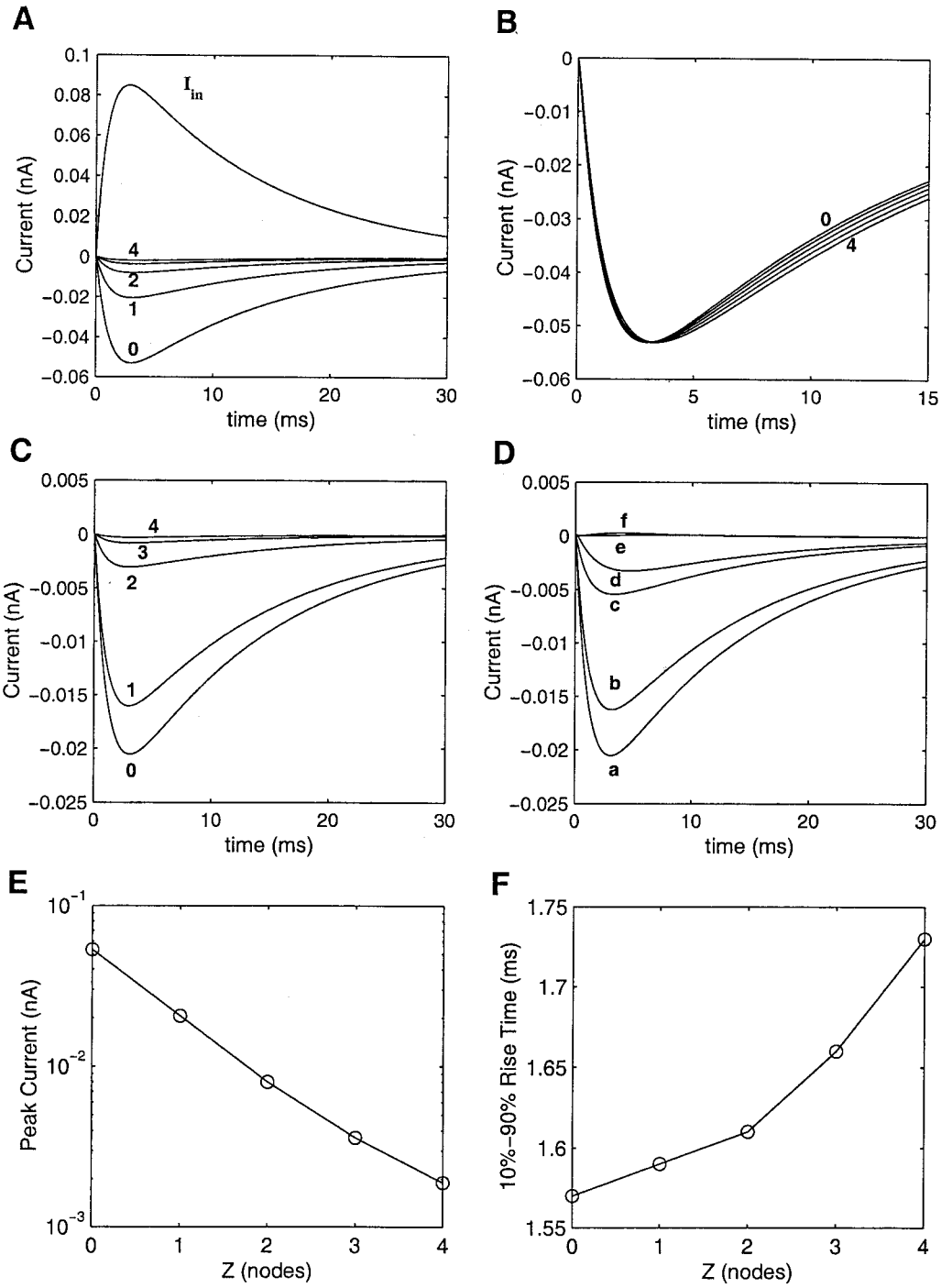

FIGURE 5 Theoretical currents measured by a loose-patch electrode placed on a muscle cell (0, 0, 0) when an ATP quantum is released from a varicosity located at different depths in the syncytium. A, shows the positive going current I_{in} that is injected into the smooth muscle cell due to the ATP quantum (see also Fig. 2 *D*); the negative going currents labeled 0, 1, 2, 3, and 4, give the currents measured by the loose patch electrode (12 μm diameter) with center at (0, 0, 0) in response to the action of an ATP quantum released from a varicosity located on muscle cells at (0, 0, k) with k = 0, 1, 2, 3, and 4, respectively. *B* shows the relative time course of the currents recorded with an electrode centered at (0, 0, 0) when these are generated at different depths in the syncytium as indicated; the amplitude of each current has been normalised to that due to a quantal release at (0, 0, 0). *C* shows recordings at (0, 0, 0) due to ATP quanta released at one smooth muscle cell deep in the syncytium (k = 1) at j = 0 and at successively more lateral positions (i = 0, 1, 2, 3, and 4, as shown). *D* shows recordings at (0, 0, 0) due to ATP quanta released at one smooth muscle cell deep in the syncytium (k = 1) and at positions (i, j, k) = (0, 0, 1), (0, A, 1), (1, A, 1), (0, B, 1), (0, 2, 1) and (0, 1, 1) for *a* to *f*, respectively (for convention regarding positions, see Fig. 2 *C*) *E* shows quantitatively the changes in the peak amplitude of the current waveform recorded by the loose patch electrode at (0, 0, 0) as a consequence of an ATP quantum being released onto muscle cells located at different depths immediately below the electrode at k = 0, 1, 2, 3, and 4, as indicated on the abscissa (log ordinate). *F* shows the 10% to 90% rise times for the same situation as in *E*. The current injection is given in Fig. 2 *D*.

cell deep in the syncytium ($k = 2$), then the peak negative currents for changes in y are substantially smaller than those at $k = 1$ and will therefore not be detected. Quantal release giving rise to negative currents that occur under the electrode will only be recorded if release occurs at the surface or one muscle cell removed from the surface, with the latter quite small compared with the former.

Theoretical transmembrane potentials generated by quantal release from a varicosity

The transmembrane potential changes that occur at a site in the syncytium following the release of a quantum of transmitter somewhere in the syncytium have also been determined. The characteristics of these potentials depends on the relative positions of the recording electrode with respect to that of the site of quantal release, as shown in Fig. 6. The largest potential transients (which experimentally are the spontaneous excitatory junction potentials, SEJPs) are recorded when the intracellular electrode is at one end of a cell and the quantal release occurs at that end (these have an amplitude of about 1.9 mV, with a 10% to 90% rise time of 2.3 ms and decay time constant of 16.7 ms, as in Fig. 6 *B*). Large potentials also occur when recording in the middle of the cell with quantal release occurring at the same point (Fig. 6 *A*). The smallest potential transients that can be recorded experimentally ($\sim$300 μV) occur when the electrode is at the centre of a cell and quantal release occurs on the cell immediately beneath it or immediately adjacent to it; Fig. 6 *D* shows such a case, with amplitude of about 300 μV, 10%–90% rise time of 4.5 ms and decay time constant of 23 ms. Spontaneous quantal release of sufficient amplitude to be measured above the noise level of about 300 μV, with a 50 MΩ intracellular electrode is then, surprisingly, almost entirely restricted to that occurring on the impaled cell.

The earliest recordings of spontaneous EJPs due to the release of ATP showed that the amplitude-frequency histogram of these was skewed rather than Gaussian (Burnstock and Holman, 1961). This was later attributed to the electrotonic propagation, into the cell recorded from, of the potential arising as a consequence of a quantum of transmitter being released elsewhere in the syncytium (Bennett, 1972). However, the above considerations suggest that most of the variations in size of the spontaneous EJPs arise from the different distances between the recording electrode and the sites of quantal release on the same cell (see Fig. 6, *A–D*). In order to see if this is the case, calculations were performed to determine the characteristics of the transmembrane potential changes arising at different sites in a single muscle cell when a quantum of transmitter is released at different sites throughout the syncytium. Fig. 6 *F* shows that there can be a decrease of as much as 60% in the amplitude of the recorded potential change within a single cell if the intracellular electrode is at one end of the cell and the quantal release is at the opposite end. On the other hand, the potentials measured at any site in a cell, when quantal release occurs at any site in adjacent cells, shows a decrease of over 75% compared to the largest potential that would be recorded if a quantal release occurred near the recording electrode in the cell under consideration (see Fig. 6, *F* and *C*). Only the largest of these potentials, which is about 400 μV (Fig. 6 *C*), would be recorded above the noise level of a 50 MΩ resistance intracellular recording electrode.

In order to make a quantitative comparison between the predictions of the theory and experimental observations on SEJPs, frequency distributions have been generated for the amplitudes of the potential changes recorded at a site in a smooth muscle cell when quantal potentials are generated at different sites in the cell and syncytium, as shown in Fig. 6. Fig. 7 *A* shows that the theoretical distribution is skewed rather than Gaussian, but does not follow a gamma distribution as does the amplitude-frequency histogram of recorded SEJPs (Bennett, 1972). Evidence has been presented previously for multiquantal release of spontaneous transmitter secretion (Bennett et al., 1996). If the input current to the syncytium consists of transients like that in Fig. 2 *D*, but with amplitudes distributed as a Poisson mixture of Gaussians, with the Gaussian at $n = 1$ having mean amplitude of 85 pA (s.d., 20 pA) and the Poisson a mean of 105 pA, then the amplitude-frequency distribution is as shown in Fig. 7 *B*. In this case, the distributions is similar to the experimental distribution, with outliers occurring at up to 5 mV. This analysis supports the previous conclusion that spontaneous release from sympathetic varicosities is multiquantal.

Comparison between the theoretical quantal currents and those recorded experimentally

Single strings of sympathetic varicosities on the surface of the mouse vas deferens have been shown to form close-contact junctions with the underlying smooth muscle cells in which the closest point of approach is less than 50 nm (Cottee et al., 1996). The varicosities in bundles of axons do not come into such close contact with the smooth muscle cells. Single strings of varicosities have been routinely identified in the present work by orthograde labeling of the varicosities with rhodamine conjugated to dextran (see Bennett et al., 1998). DiOC2(5) labeling of varicosities has also been used, but as this relies on the relative high density of DiOC2(5)-stained mitochondria in the varicosities compared with that in the muscle (Macleod et al., 1994), it is not as reliable as the rhodamine staining. We have already shown that the rhodamine labeling provides sufficient resolution to distinguish varicosities that are separated by only 500 nm (Bennett et al., 1998).

Loose patch electrodes of about 12 μm diameter were placed over strings of varicosities. Recordings of the electrode potentials due to the electrode currents arising on

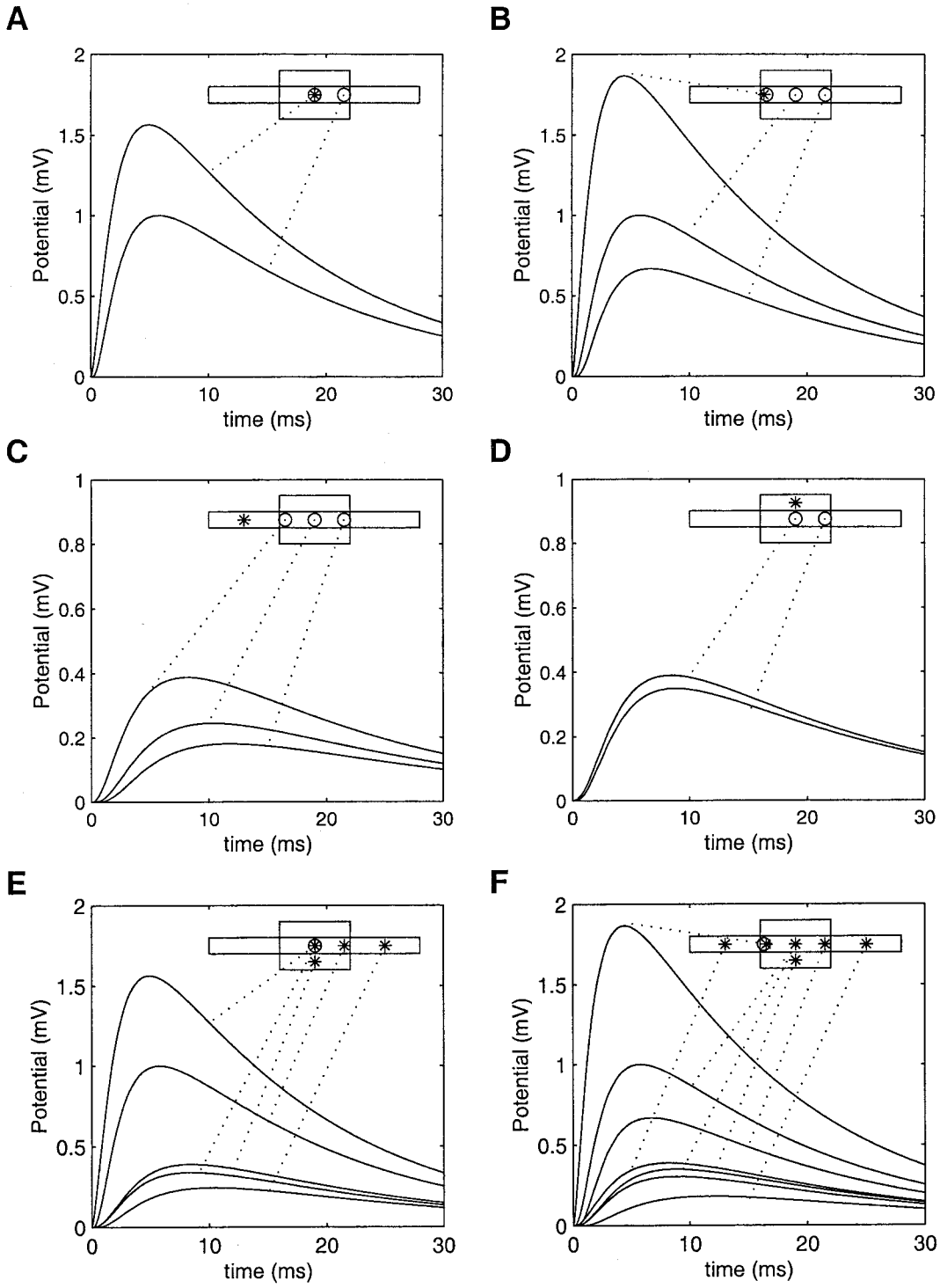

FIGURE 6 Theoretical transmembrane potential changes recorded with an intracellular electrode at the center of a surface smooth muscle cell (0, 0, 0) and at its ends [(0, P, 1) and (0, −P, 1)] when current injection simulating the release of a quantum of ATP occurs at different sites in the syncytium. In each case, the central rectangle represents the cell centered on (0, 0, 0) and the four adjoining rectangles represent the abutting cells, two in the transverse direction (x-direction) and two in the longitudinal direction (y-direction); all are in the plane $z = 0$. The center of the electrode is indicated by an open circle (○) and the release point by an asterisk (*), with the *dotted lines* indicating the corresponding potential curve. The release sites in *A, B, C,* and *D* are, respectively, at (0, 0, 0), (0, −P, 0), (−1, 0, 0) and (1, 0, 0). In *E*, the electrode is centered at (0, 0, 0) with release sites at (0, 0, 0), (0, P, 0), (0, 1, 0) and (−1, 0, 0). In *F* the electrode is at (−P, 0, 0) with release occurring at (−1, 0, 0), (−P, 0, 0), (0, 0, 0), (0, P, 0), (0, 1, 0), (−1, 0, 0), and (0, 0, −1).

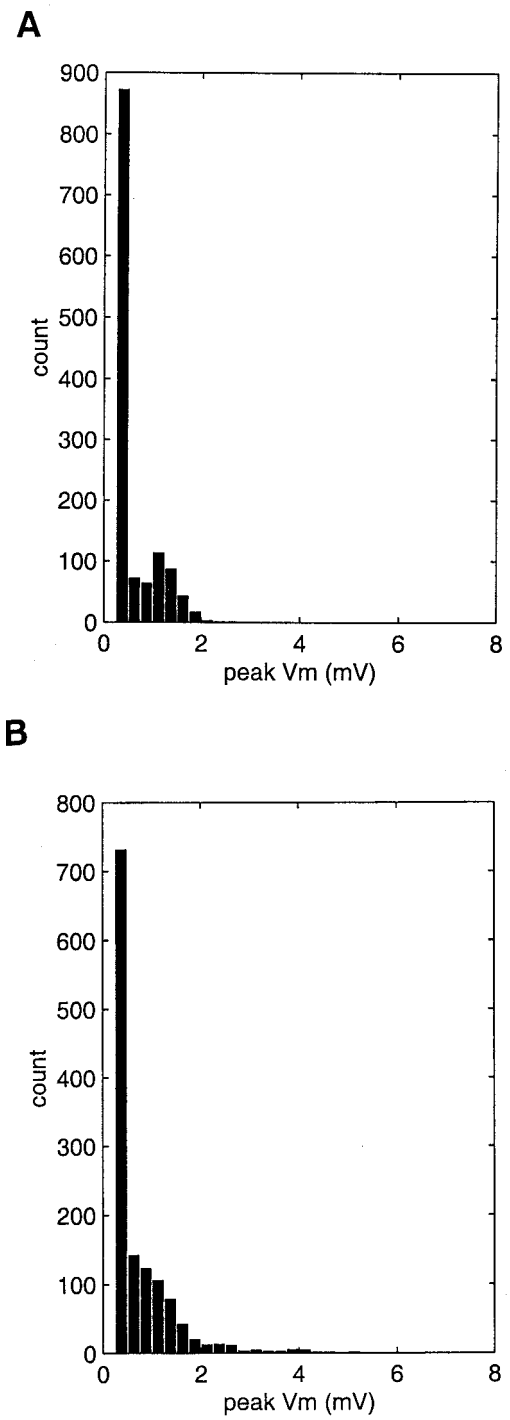

FIGURE 7 Theoretical determinations of the amplitude-frequency histograms of spontaneous EJPs. The distributions were obtained by considering EJPs generated as in Fig. 6, *C* and *F*, with the input currents drawn from a Gaussian distribution (mean 85 pA, s.d. 20 pA) as in *A*, or as a Poisson (mean, 105 pA) mixture of such Gaussians, as in *B*. The noise level has been taken as 0.5 mV.

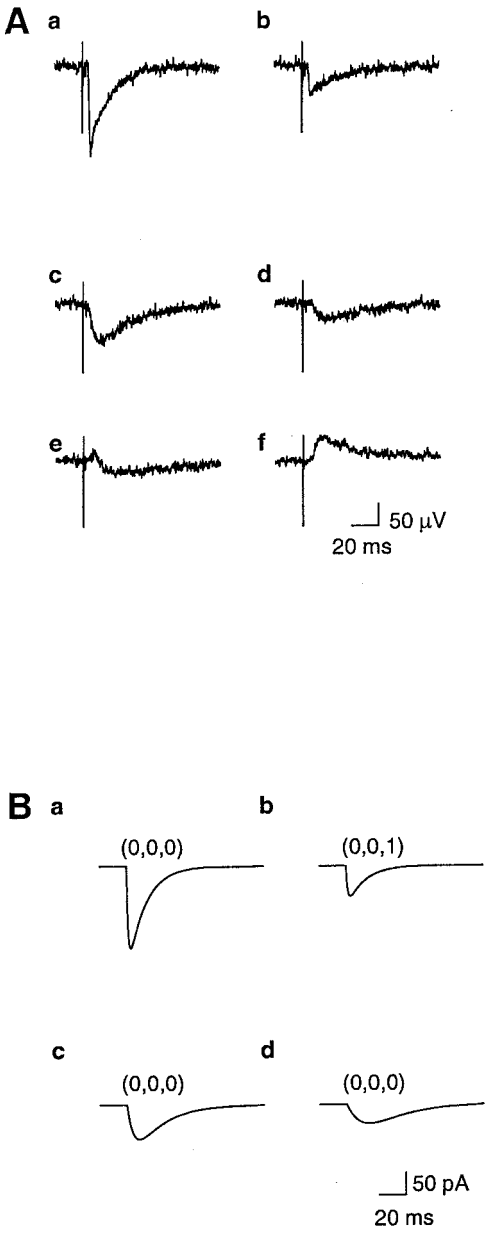

FIGURE 8 Comparison between experimental (*A*) and theoretical (*B*) determinations of the currents measured by a loose-patch electrode placed on a varicosity. *A*: (a) and (b) show fast rise-time EJCs of small and large amplitude; (c) and (d) show slow rise-time EJCs of small amplitude; (e) and (f) show EJCs with positive components. *B*: (a) and (b) show fast rise-time EJCs of small and large amplitude. The numbers in parenthesis refer to the node position at which the quantum of ATP was released. (c) and (d) give simulated current generated with rise times drawn from a Gaussian distribution (mean 10 ms, s.d. 4.4 ms) and amplitudes from a Poisson (mean 38 pA) mixture of Gaussians (mean 35 pA, s.d. 7 pA).

stimulation of the sympathetic nerves showed that these fell into two broad categories: the majority were purely negative going EJCs (Fig. 8 *A*, a–d) with a minority consisting of either purely positive going EJCs (Fig. 8Af) or consisting of an early positive going component followed by a negative going component (Fig. 8 *A*e). The purely negative EJCs possessed different amplitudes and time courses characterised by their different times to peak (measured by the 10% to 90% rise time, T_p), with both large and small potentials

having short T_p values (Fig. 8 *A*, a and b) and many small EJCs having long T_p values (Fig. 8 *A*, c and d).

Plots of T_p versus amplitude for the EJCs measured using a 12-μm diameter loose patch electrode placed over a visualized varicosity string are shown in Fig. 9 *A*; the noise level using an approximately 1 MΩ seal resistance is about 15 to 20 μV. The distribution of points is approximately boomerang-shaped, with predominant vertical and horizontal arms. If the loose patch electrode was not placed over a visualized string of varicosities but rather over a region where bundles of axons were evident then the recorded EJCs were of small amplitude, disappearing into the noise level and possessing long T_p values (see Fig. 8 A, c and d). Plots of T_p versus amplitude for these EJCs gave points contained in an envelope that occupied a predominantly vertical orientation (Fig. 9 *B*), with no horizontal limb as in Fig. 9 *A*.

Theoretical EJCs, similar to those recorded experimentally, can easily be generated in the syncytium by injecting the current of Fig. 2 *D* and determining the currents recorded by a loose-patch electrode at the site of the simulated quantal release or elsewhere (compare Fig. 8 *B*, a and b, with Fig. 8 *A*, a and b). However, it has already been shown that sympathetic varicosities are likely to secrete multiquantally (see Fig. 7; for a review, see Bennett, 1996). This being the case, each node in the distributed representation of muscle cells in the syncytium was given the capacity to receive a multiquantal input, consisting of a Poisson mixture of Gaussians in which the Poisson had mean 105 pA and the Gaussian had mean 85 pA and standard deviation 20 pA. Furthermore, there is a stochastic variation in the time course of the quantal currents that arises from the stochastic nature of the interaction of transmitter quanta with a receptor patch (see fig. 8 in Bennett et al., 1995). In order to accommodate this fact in the simulations, the times to peak for the injected currents were chosen stochastically from a gamma distribution [density function $f(x) = (\lambda/\Gamma(r))(\lambda x)^{r-1}\exp(-\lambda x)$] with parameters $r = 3$ and $\lambda = 1.76$ ms^{-1}, with the time origin displaced to 1.1 ms so that no rise time is shorter than 1.1 ms. The mean rise time is thus $1.1 + r/\lambda = 2.8$ ms. (In the computations, these amplitudes and rise times were implemented by keeping $\alpha = 0.08$ ms^{-1} in Eq. 12 and adjusting I_0 and β.) The plot of T_p versus amplitude of the predicted currents, recorded with a 12-μm diameter loose patch electrode when quantal currents possessing the characteristics described above are generated at nodes throughout the syncytium, is shown in Fig. 9 *C*. The points generated in this way occupy an envelope that is oriented horizontally, with no indication of the boomerang-shaped envelope of points observed experimentally (compare Fig. *C* with Fig. 9 *A*). (If the value of the seal resistance is 1 MΩ, then a direct comparison can be made between the experimental and theoretical predictions given in Fig. 9, as the scalings of the abscissa giving currents can be converted to voltages by multiplying by the 1 MΩ resistance.)

Nearly all of the points that are generated by simulated quantal releases onto muscle cells, other than those immediately beneath the loose-patch electrode, fall into the noise level to the left of the vertical broken line in Fig. 9 *C*. This is emphasized in Fig. 9 *D*, which shows only the points for simulated EJCs that do not arise immediately beneath the electrode; the few EJCs that are to the right of the vertical broken line arise from the muscle cell under the electrode that is one removed from the surface (that is, at $k = 1$). The syncytium ensures that the diminution in size of the EJCs is not accompanied by much change in their temporal characteristics. It appears likely that the horizontal limb of points in the experimental plots of T_p versus amplitude (as in Fig. 9 *A*) arises predominantly from quantal release onto the muscle cells immediately beneath the loose-patch electrode.

The source of the transmitter that gives rise to the slow and small EJCs, indicated by the vertical limb of points in Fig. 9 *A*, is not known so there are no theoretical grounds for determining their characteristics. We have therefore simulated them by the injection of appropriate currents. Currents with long rise times drawn from a Gaussian distribution (mean 10 ms, standard deviation 4.4 ms) and small amplitudes drawn from a Poisson (mean 38 pA) mixture of Gaussians (mean 35 pA, standard deviation 7 pA) were used in the simulation (the value $\alpha = .05$ ms^{-1} was also used in Eq. 12), giving currents of the type shown in Fig. 8 *B*, c and d, and the results shown in Fig. 9 *F* (and, with the noise removed, Fig. 9 *H*). Most of the points are in the noise (to the left of the vertical line) with the remainder forming a limb of points characterizing EJCs that would be recorded. Putting together the results of injecting both fast as well as small and slow currents gives the results of Fig. 9 *E* (or, with the noise removed, Fig. 9 *G*), which is the complete simulation of the experimental results of Fig. 9 *A*.

A further test of the idea that the slow components of transmission arise by a different mechanism than the fast components is to perfuse the 12 μm loose patch electrode with a solution that differentially blocks the fast components. The present theory suggests that the fast component is due to classical quantal transmission and therefore should be blocked by agents that interfere with the process of exocytosis involving the vesicle-associated proteins (Südhof, 1995). In order to test this experimentally, we have perfused the loose-patch electrode with penetratin disulphide linked to a peptide of α-SNAP, a domain that is known to block classical transmitter exocytosis (de Bello et al., 1995). As explained in Methods, penetratin is a carrier peptide that releases the peptide of α-SNAP once it enters the cells beneath the loose-patch electrode because of the change in redox potential of the intracellular milieu. Fig. 10 shows the effects of perfusing the recording electrode in this way: before perfusion with penetratin/α-SNAP peptide, the recordings of EJCs provided the usual boomerang-shaped envelope of points on the T_p versus amplitude graph (Fig. 10 *A*); however, no fast EJCs were recorded after perfusion

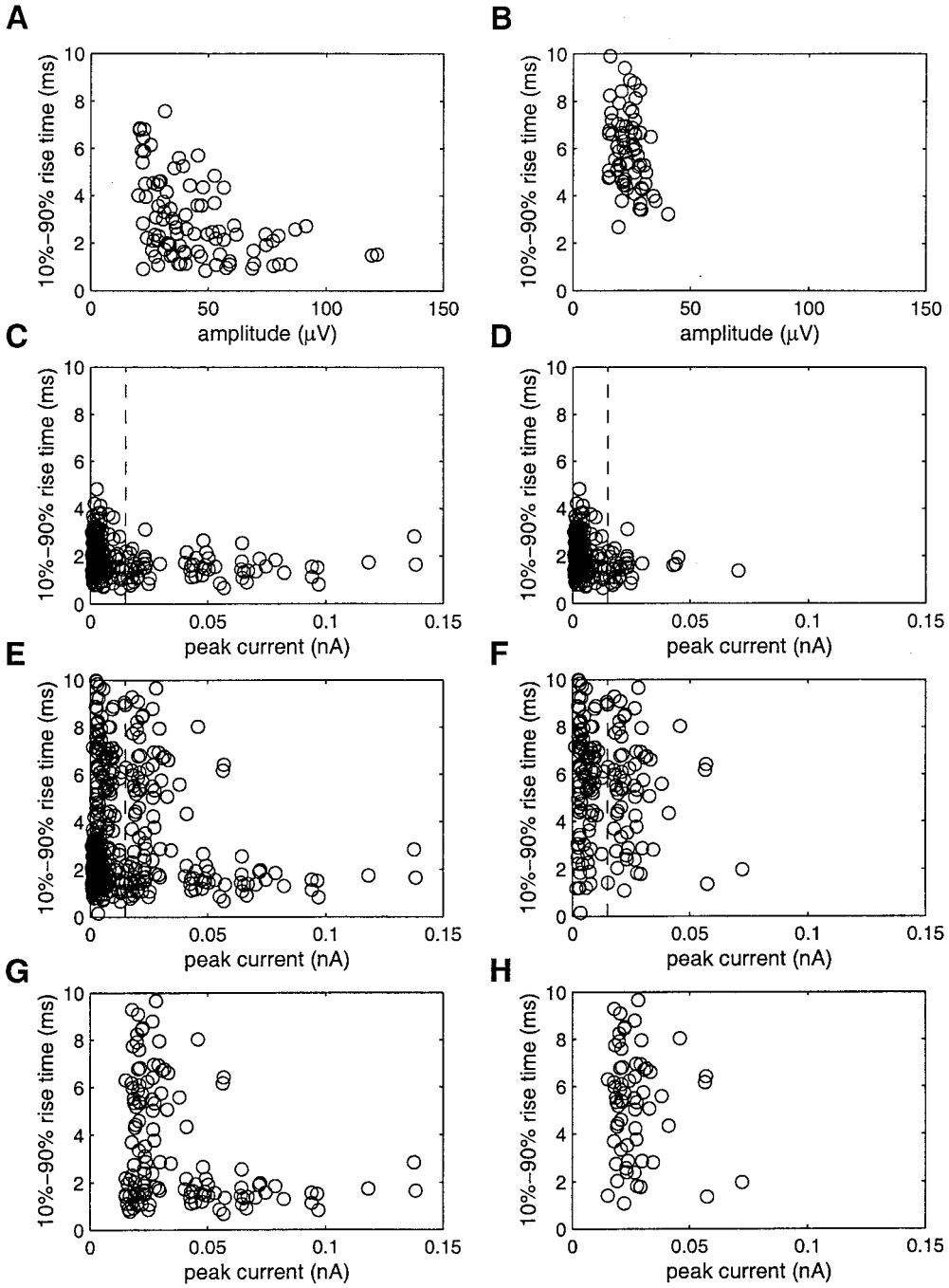

FIGURE 9 Comparison between theoretical and experimental determination of the rise time and amplitude of negative-going currents recorded with a loose-patch electrode (12 μm diameter) following evoked quantal release from varicosities throughout the muscle syncytium. *A*, experimental rise time/amplitude characteristics of currents recorded by an electrode positioned over two visualized varicosities during stimulation with 120 pulses at 0.1 Hz. *B*, experimental characteristics of currents recorded by an electrode placed at a position on the muscle at which no strings of varicosities were observed. *C*, theoretical rise time/amplitude characteristics of currents recorded with a 12 μm diameter loose-patch electrode when quantal release occurred with the same probability from all varicosities (one per node). The quantal release was simulated by an input current with amplitude drawn from a Poisson (mean 105 pA) mixture of Gaussians (mean 85 pA, standard deviation 20 pA) and time to peak drawn from a gamma distribution (parameters $r = 3$, $\lambda = 1.76$, origin displaced to 1.1 ms). The vertical broken line indicated the noise level if a 1 MΩ loose-patch is formed. *D*, the same as for *C* except contributions from varicosities at the surface of the muscle (i.e., $z = 0$) have been removed; this indicates that most of the recordable currents come from varicosities at the surface; vertical broken line as for *C*. *E*, theoretical rise time/amplitude of currents generated by the simulations in *C* and *F* cumulatively; compare with experimental data in *A*. *F*, theoretical rise time/amplitude of the currents that arise when the loose-patch electrode records from sites at which no strings of varicosities can be observed on the surface of the muscle (as in *B*). Each node received injection of a current with amplitude drawn from a Poisson (mean 38 pA) mixture of Gaussians (mean 35 pA, standard deviation 7 pA) and a time to peak drawn from a Gaussian distribution (mean 10 ms, standard deviation 4.4 ms). *G* and *H* are the same as *E* and *F* but with the values falling in the noise level (that is, points to the left of the broken line) removed.

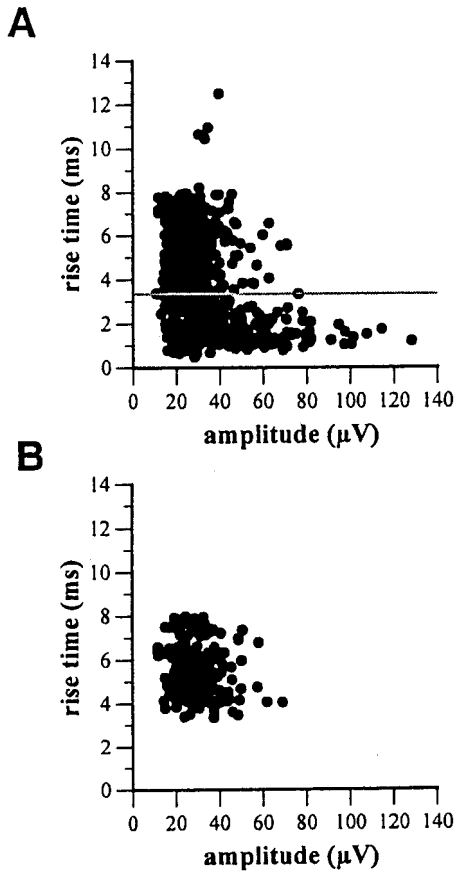

FIGURE 10 Experimental observations on the effects of blocking quantal transmitter release on the characteristics of EJCs. *A* shows the rise time/amplitude characteristics of EJCs recorded with a 12 μm loose-patch electrode. *B* shows the characteristics of EJCs recorded with the same electrode after it had been perfused with an α-SNAP peptide-penetratin complex for 20 min. The horizontal line in *A* indicates the position below which no EJCs with those characteristics were recorded.

with the peptide, so that the horizontal limb of the boomerang-shaped envelope of points was removed (Fig. 10 *B*). This was the case in all 12 experiments performed. These observations support the conclusion of the theoretical section that the fast and slow EJCs arise by different mechanisms, and that the latter is not a consequence of the quantal release of transmitter.

Comparison between the theoretical quantal transmembrane potentials and those recorded experimentally

We have previously shown that it is not possible to predict the stochastic variations in the time course of excitatory junction potentials (EJPs) from impulse to impulse without recourse to the idea that transmitter release onto smooth muscle cells occurs both by means of occasional quantal releases, each giving rise to fast potential changes in the cells, as well as by means of a relatively large number of small and slow releases that give rise to slow potential changes (see Introduction; Bennett and Gibson, 1995). The above analysis of EJCs confirms this conclusion. In order to test it further, however, it is necessary to perform experiments in which either the fast or slow components of transmission are depressed, leaving the other exposed. Recently, Manchanda and Venkateswarlu (1999) provided this evidence by showing that the alcohol agent heptanol differentially blocks the slow component of the EJP, leaving just the fast component which thus has the characteristics of a spontaneous EJP, that is, the characteristics of EJPs obtained by injecting a current like that in Fig. 2 *D* into a node of the syncytium giving rise to potentials shown in Fig. 7. These observations themselves offer credence to the present analysis which points to two different sources of transmitter. We have examined our theory of transmission from sympathetic nerves to see if it can predict the experimental observations using heptanol.

The mixture of fast and slow components of transmission (with characteristics given by both the horizontal and vertical arms of the rise time/amplitude distribution in Fig. 9 *E*) give the simulated EJC of Fig. 11 *B*a, which may be compared with the experimental EJC of Fig. 11 *A*a; removal of successively larger amounts of the slow component of transmission (with characteristics similar to those given by the vertical limb of points in Fig. 9 *F*) gives the fast simulated EJP of Fig. 11 *B*, a–d, which may be compared with the experimental EJP in heptanol of Fig. 11 *A*, a–d. The preferential decrease in the probability of the slow component compared with the fast component in heptanol supports the fact that they arise by different mechanisms and that the slow one is not simply a consequence of radiation through the syncytium of the fast component from its origins. Furthermore, these simulations indicate that the persistent slow component of the EJP arises from the large number of small and slow releases detected with an extracellular electrode.

DISCUSSION

Quantal transmission from synaptic varicosities in an electrical syncytium in a volume conductor

Solution of the problem of current flow in the volume conductor surrounding a smooth muscle following the release of a quantum of transmitter at a particular site at the surface or in the depths of the muscle, provided in the present work, allows for a quantitative account of the relation between the extracellular current and the underlying conductance change. Two points emerge from this solution. First, an extracellular electrode is unlikely to be able to measure the extracellular potential field due to a quantal release, even one that occurs at the surface of the muscle, as the field strength is at most a few microvolts. It is therefore necessary to use a loose patch electrode to concentrate the current lines under the electrode and thus increase the

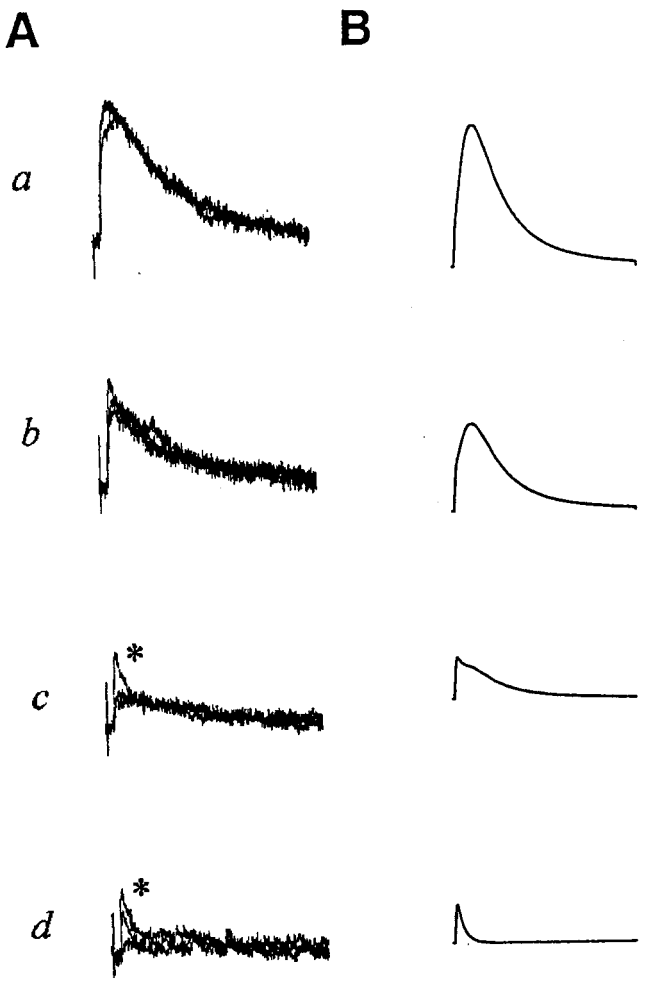

FIGURE 11 Comparison between theoretical and experimental determinations of the amplitude and time course of excitatory junction potentials (EJPs) recorded with an intracellular electrode under conditions where the small and slow currents do not contribute to generation of the EJP. *A* shows experimental results when the slow persistent phase of the EJP is gradually blocked, (a) to (d), revealing only a fast stochastic phase (*asterisk*) on exposure of the preparation to heptanol (data from fig. 1 in Manchanda and Venkateswarlu, 1999). *B* shows in (a) theoretical generation of the EJP in a cell due to injecting into the syncytium small and slow currents of the types with the characteristics given in Fig. 9 *F*, together with occasional relatively large and fast currents of the types with the characteristics given in Fig. 9 *C*; parts (b) to (d) show the effects of gradually reducing to zero the number of small and slow currents injected into the syncytium.

potential field in the vicinity of the electrode to values in excess of about 15 μV. The second point to emerge from this work is that the T_p of the extracellular current measured in the volume conductor does not increase much as the amplitude (I_e) decreases, for quantal releases at increasing depths along the z-axis in the muscle beneath the electrode. Thus, the relation between rise times and amplitude of synaptic currents that has been used traditionally to determine the site of synaptic current generation in dendritic neurons (Rall et al., 1992) cannot be used to determine the site of junctional current generation in a syncytium. A previous bidomain description of the electrical syncytium also showed a steep decrease in the amplitude of the quantal currents measured at the surface which originate at increasing depths in the syncytium (see fig. 7 in Bennett et al., 1993), but as this work did not provide a solution to the problem of measuring with a loose patch electrode the quantal current flowing in a volume conductor and also used an artificially constrained choice of intracellular and interstitial resistances, it overestimated the extent of the amplitude decrease and that of the time to peak increase with depth of origin of the current in the syncytium (compare fig. 7 in Bennett et al. (1993) with Fig. 5 in the present work).

Spontaneous quantal currents measured with a loose-patch electrode have been reported that have T_p values of 4.3 ± 1.5 ms with many of these having amplitudes in excess of 0.2 nA (Åstrand et al., 1988). Given that the loose-patch electrode has a resistance when recording of about 1.0 MΩ, then the amplitudes of these quantal currents are less than about 150 μV, as observed in the present work. As evoked EJCs have been observed with similar amplitudes and time courses to spontaneous EJCs, it has been suggested that quantal currents arising from a particular site in the syncytium can be identified by their characteristic size and temporal characteristics, called fingerprints, thus allowing for estimates to be made of the probability of secretion from particular sites (with probabilities of about 0.005 to 0.8 in the guinea-pig vas deferens, Brock and Cunnane (1988), and about 0.002 to 0.02 in the rat tail artery, Åstrand and Stjärne (1989)). However, it has been argued that the characteristics of an EJC generated at a particular site in the syncytium can arise from stochastic fluctuations at the site of exocytosis rather than from differences in the position of the varicosity in the syncytium (Henery et al., 1998). The argument that evoked EJCs possessing particular characteristics tend to occur in clusters during a train has been taken as further evidence for varicosities at particular sites in the syncytium giving rise to currents at the surface of a kind that characterise that site; however, analysis of these trains does not supply objective evidence for clustering (Karunanithi et al., 1995). In the present work, it has been shown both experimentally and theoretically that the evoked EJCs arising from surface varicosities beneath a loose patch electrode all have short rise times, in the range from about 1.0 to 3.0 ms, and that those EJCs which arise from quantal release due to varicosities located one muscle cell deep from the surface mostly have rise times in the same range. The amplitude of the smallest EJCs recorded from the surface varicosities is about the same as the largest of those arising from varicosities that are a muscle cell deep if a 12-μm diameter loose-patch electrode is used. With a 4-μm diameter electrode, the size of the contributions from varicosities not at the surface is negligible compared with those at the surface.

The present observations indicate that there is multiquantal secretion, which can be described by a Poisson distribu-

tion, from each of the two or three varicosities visualized beneath a loose patch electrode. Multiquantal release from varicosities has previously been argued to be the case on the basis of a statistical analysis of the amplitude-frequency histograms of spontaneous EJCs recorded with 4-μm diameter loose-patch electrodes (Bennett et al., 1996). In this work, the amplitude-frequency histograms of spontaneous EJCs were also described by a Poisson distribution, providing independent evidence for multiquantal release from varicosities. This suggests that the large range of amplitudes of SEJPs, recorded with an intracellular electrode, arises from the multiquantal nature of the unit of ATP secreted. The alternative explanation is that they arise as a consequence of electrotonic radiation into the recorded cell of the results of monoquantal release from varicosities elsewhere in the muscle, as originally suggested (Bennett, 1972). However the present work shows that this is not possible, as the theoretical frequency histogram of spontaneous EJP amplitudes recorded from a muscle cell on the surface of a syncytium in a volume conductor does not give rise to the observed amplitude-frequency histograms. In order to achieve this agreement it is necessary to have multiquantal spontaneous quantal release, as has been observed at a number of other synapses (see, for example, Bennett, 1995).

Non-quantal transmission from sympathetic nerves in an electrical syncytium in a volume conductor

The present analysis shows that it is not possible to generate small EJCs with long rise times as a consequence of the radiation under the loose patch recording electrode of the results of a quantum being released elsewhere in the syncytium. It has previously been shown that it is not possible to generate the persistent slow component of the EJP by means of the radiation of quantal currents from elsewhere in the syncytium into the cell recorded from with an intracellular electrode (Bennett and Gibson, 1995). This latter study showed that the slow and persistent phase of the EJP could be described if a relatively large number of small and slow conductance changes occurred in each cell; the fast and stochastic phase of the EJP was then attributed to a single large conductance change due to the release of a quantum onto the impaled cell. The present analysis of the EJCs show that these can likewise be divided into two independent types, namely quantal relatively large and fast and non-quantal small and slow, with the latter very likely giving rise to the persistent component of the EJPs.

The question arises as to the origins of these small and slow EJCs. Such EJCs could be recorded, in the absence of fast EJCs, when the loose-patch electrode was perfused with an exocytosis-blocking peptide of α-SNAP. These observations indicate that, whatever the source of the transmitter, it appears to be released in a non-quantal fashion. In the present case, the transmitter for both quantal and non-quantal release is ATP as both the persistent and stochastic components of the EJP are completely blocked by the antagonist suramin as well as by desensitization with α,β-methylene ATP (Sneddon and Westfall, 1984). In addition, gene deletion of the purinergic receptor P_{2x1} also leads to the disappearance of the EJP and of spontaneous EJPs (Mulryan et al., 2000).

Recent evidence has shown that the axons of dorsal ganglion cells can release ATP along their length, and that this ATP can activate cellular processes in surrounding Schwann cells (Stevens and Fields, 2000). It is not known if this release occurs via a classical calcium-dependent exocytotic mechanism or not. If it does not, and if such ATP release also occurs along the length of sympathetic nerves, then such ATP secretions could explain the existence of the non-quantal EJCs observed in the present work. It has recently been argued that the SNARE (soluble NEM-sensitive factor attachment protein receptors) hypothesis for vesicle docking and fusion (Südhof, 1995; Rothman, 1994) might not apply uniformly to all exocytotic secretory processes, a fact that is known to be the case for large and small dense-core vesicles, but that might also hold for different transmitter-containing small vesicles (Langley and Grant, 1997; Zimmerman, 1997). Other sources of evoked transmitter release that do not use a classical exocytotic mechanism include muscle cells themselves, for myocytes can secrete acetylcholine (Dan and Poo, 1992; Fu et al., 1998) and Schwann cells may also secrete transmitter (Jeftinija and Jeftinija, 1998). Also, nerves can secrete transmitter through a potential-dependent transporter (Schwartz, 1987; O'Malley et al., 1992). None of these sources of transmitter is excluded by the present experimental results. It will be of interest to determine the secretory process involved in generating the slow EJCs.

This work was supported by Australian Research Council (ARC) grant A10009315 and also by an ARC institutional grant.

REFERENCES

Åstrand, P., and L. Stjärne. 1989. On the secretory activity of single varicosities in the sympathetic nerves innervating the rat tail artery. *J. Physiol.* 409:207–220.

Åstrand, P., J. A. Brock, and T. C. Cunnane. 1988. Time course of transmitter action at the sympathetic neuroeffector junction in rodent vascular and non-vascular smooth muscle. *J. Physiol.* 401:657–670.

Barden, J. A., L. J. Cottee, and M. R. Bennett. 1999. Vesicle-associated proteins and P2x receptor clusters at single sympathetic varicosities in mouse vas deferens. *J. Neurocytol.* 24:469–480.

Bennett, M. R. 1972. Autonomic neuromuscular transmission. Monographs of the Physiological Society. Cambridge University Press, Cambridge, UK.

Bennett, M. R. 1973. Structure and electrical properties of the autonomic neuromuscular junction. *Phil. Trans. Roy. Soc. Lond.* B265:25–34.

Bennett, M. R. 1995. The origin of Gaussian distributions of synaptic potentials. *Prog. Neurobiol.* 46:331–350.

Bennett, M. R. 1996. Autonomic neuromuscular transmission at a varicosity. *Prog. Neurobiol.* 50:505–532.

Bennett, M. R., and N. C. R. Merrillees. 1966. On analysis of the transmission of excitation from autonomic nerves to smooth muscle. *J. Physiol.* 185:520–535.

Bennett, M. R., W. G. Gibson, and R. R. Poznanski. 1993. Extracellular current flow and potential during quantal transmission from varicosities in a smooth muscle syncytium. *Phil. Trans. Roy. Soc. Lond. B.* 342: 89–99.

Bennett, M. R., and W. G. Gibson. 1995. On the contribution of quantal secretion from close-contact and loose-contact varicosities to the synaptic potentials in the vas deferens. *Phil. Trans. Roy. Soc. Lond. B.* 347:187–204.

Bennett, M. R., L. Farnell, W. G. Gibson, and S. Karunanithi. 1995. Quantal transmission at purinergic junctions: stochastic interaction between ATP and its receptors. *Biophys. J.* 68:925–935.

Bennett, M. R., J. Robinson, M. C. Phipps, S. Karunanithi, Y. Q. Lin, and L. Cottee. 1996. Quantal components of spontaneous excitatory junction potentials at visualised varicosities. *J. Autonom. Nerv. Sys.* 56:161–174.

Bennett, M. R., L. Farnell, W. G. Gibson, and N. A. Lavidis. 1997. Synaptic transmission at visualized sympathetic boutons: stochastic interaction between acetylcholine and its receptors. *Biophys. J.* 72: 1595–1606.

Bennett, M. R., A. Cheung, and K. L. Brain. 1998. Sympathetic neuromuscular transmission at a varicosity in a syncytium. *Micros. Res. Tech.* 42:433–450.

Bennett, M. R., L. Farnell, W. G. Gibson, G. T. Macleod, and P. Dickens. 2000. Quantal potential fields around individual active zones of amphibian motor-nerve terminals. *Biophys. J.* 78:1106–1118.

Blakeley, A. G., and T. C. Cunnane. 1979. The packeted release of transmitter from the sympathetic nerves of the guinea-pig vas deferens: an electrophysiological study. *J. Physiol.* 296:85–96.

Brink, P. R. 1998. Gap junctions in vascular smooth muscle. *Acta. Physiol. Scand.* 164:349–356.

Brock, J. A., and T. C. Cunnane. 1987. Relationship between the nerve action potential and transmitter release from sympathetic postganglionic nerve terminals. *Nature.* 326:605–607.

Brock, J. A., and T. C. Cunnane. 1988. Electrical activity at the sympathetic neuroeffector junction in the guinea pig vas deferens. *J. Physiol.* 399:607–632.

Burnstock, G., and M. E. Holman. 1961. The transmission of excitation from autonomic nerve to smooth muscle. *J. Physiol.* 155:115–133.

Cole, K. S., and H. J. Curtis. 1950. Bioelectricity: electric Physiology. *In* Medical Physics, vol. 2. O. Glasser, ed. The Year Book Publisher, Chicago.

Cottee, L. J., N. A. Lavidis, and M. R. Bennett. 1996. Spatial relationships between sympathetic varicosities and smooth muscle cells in the longitudinal layer of the mouse vas deferens. *J. Neurocytol.* 25:413–425.

Dan, Y., and M. M. Poo. 1992. Quantal transmitter secretion from myocytes loaded with acetylcholine. *Nature.* 359:733–736.

DeBello, W. M., V. O'Connor, T. Dresbach, S. W. Whiteheart, S. S. Wang, F. E. Schweizer, H. Betz, J. E. Rothman, and G. J. Augustine. 1995. SNAP-mediated protein-protein interactions essential for neurotransmitter release. *Nature.* 373:626–630.

Fu, W. M., H. C. Liou, Y. H. Chen, and S. M. Wang. 1998. Release of acetylcholine from embryonic myocytes in Xenopus cell cultures. *J. Physiol.* 509:497–506.

Henery, R., W. G. Gibson, and M. R. Bennett. 1997. Quantal currents and potential in the three-dimensional anisotropic bidomain model of smooth muscle. *Bull. Math. Biol.* 59:1047–1075.

Henery, R., J. Robinson, and M. R. Bennett. 1998. Methods for grouping shapes of synaptic currents recorded from sets of synapses. *J. Neurosci. Meth.* 86:79–90.

Henriquez, C. S. 1993. Simulating the electrical behaviour of cardiac tissue using the bidomain model. *Crit. Rev. Biomed. Eng.* 21:1–77.

Jeftinija, S. D., and K. V. Jeftinija. 1998. ATP stimulates release of excitatory aminoacids from cultured Schwann cells. *Neuroscience.* 82: 927–934.

Karunanithi, S., M. C. Phipps, J. Robinson, and M. R. Bennett. 1995. Statistics of quantal secretion during long trains of sympathetic nerve impulses in mouse vas deferens. *J. Physiol.* 489:171–181.

Krassowska, W., and J. C. Neu. 1994. Effective boundary conditions for syncytial tissues. *IEEE Trans. Biomed. Eng.* 41:143–150.

Langley, K., and N. J. Grant. 1997. Are exocytosis mechanisms neurotransmitter specific? *Neurochemistry International.* 31:739–757.

Lavidis, N. A., and M. R. Bennett. 1992. Probabilistic secretion of quanta from visualized sympathetic nerve varicosities in mouse vas deferens. *J. Physiol.* 454:9–26.

Lavidis, N. A., and M. R. Bennett. 1993. Probabilistic secretion of quanta from visualized varicosities along single sympathetic nerve terminals. *J. Aut. Nerv. System.* 43:41–50.

MacLeod, G., N. A. Lavidis, and M. R. Bennett. 1994. Calcium dependence of quantal secretion from visualized sympathetic nerve varicosities on the mouse vas deferens. *J. Physiol.* 480:61–70.

Manchanda, R., and K. Venkateswarlu. 1999. Quantal evoked depolarizations underlying the excitatory junction potential of the guinea-pig vas deferens. *J. Physiol.* 520:527–537.

Mulryan, K., D. P. Gitterman, C. J. Lewis, C. Vial, B. J. Leckie, A. L. Cobb, J. E. Brown, E. C. Conley, G. Buell, C. A. Pritchard, and R. J. Evans. 2000. Reduced vas deferens contraction and male infertility in mice lacking P_{2x1} receptors. *Nature.* 403:86–89.

O'Malley, D. M., J. H. Sandell, and R. H. Masland. 1992. Co-release of acetylcholine and GABA by the starburst amacrine cell. *J. Neurosci.* 12:1394–1408.

Prochiantz, A. 1999. Homeodomain-derived peptides: in and out of the cells. *Ann. New York Acad. Sci.* 886:172–179.

Purves, R. D. 1976. Current flow and potential in a three-dimensional syncytium. *J. Theoret. Biol.* 60:147–162.

Rall, W., R. E. Burke, W. R. Holmes, J. J. Jack, S. Redman, and I. Segev. 1992. Matching dendritic neuron models to experimental data. *Physiol. Rev.* 72:S159–S186.

Roth, B. J. 1992. How the anisotropy of the intracellular and extracellular conductivities influences stimulation of cardiac muscle. *J. Math. Biol.* 30:633–646.

Rothman, J. E. 1994. Mechanisms of intracellular protein transport. *Nature.* 372:55–63.

Schwartz, E. A. 1987. Depolarization without calcium can release gamma-aminobutyric acid from a retinal neuron. *Science.* 238:350–355.

Sneddon, P., and D. P. Westfall. 1984. Pharmacological evidence that adenosine triphosphate and noradrenaline are co-transmitters in the guinea-pig vas deferens. *J. Physiol.* 347:561–580.

Stevens, B., and R. D. Fields. 2000. Response of Schwann cells to action potentials in development. *Science.* 287:2267–2271.

Südhof, T. C. 1995. The synaptic vesicle cycle: a cascade of protein-protein interactions. *Nature.* 375:645–653.

Zimmermann, H. 1997. Are mechanisms of exocytosis neurotransmitter specific? *Neurochem. Int.* 31:759–761.